Experimental Thermal and Fluid Science 85 (2017) 119–131

Contents lists available at ScienceDirect

Experimental Thermal and Fluid Science

journal homepage: www.elsevier.com/locate/etfs

Integrated flat heat pipe with a porous network wick for high-heat-flux electronic devices

Xianbing Ji [a], Hongchuan Li [a], Jinliang Xu [a,*], Yanping Huang [b]

[a] The Beijing Key Laboratory of Multiphase Flow and Heat Transfer, North China Electric Power University, Beijing 102206, PR China
[b] CNNC Key Laboratory on Nuclear Reactor Thermal Hydraulics Technology, Nuclear Power Institute of China, Chengdu 610213, PR China

ARTICLE INFO

Article history:
Received 25 May 2016
Received in revised form 23 January 2017
Accepted 3 March 2017
Available online 6 March 2017

Keywords:
Integrated
Flat heat pipe
Copper foam
Porous network wick

ABSTRACT

A novel integrated flat heat pipe (IFHP) was constructed, which consists of an evaporator and a condenser with multiple channels fabricated in the fin heat sink. A layer of compressed copper foam was sintered on the inner surface of the evaporator bottom plate, and many copper foam bars were inserted into the channels, both of which formed a porous network wick. Experiments were performed under three inclination angles (θ = 0°, 90°, and 180°), using acetone as the working fluid. Air and water cooling methods were used to cool the fin heat sink. Compared with the conventional flat heat pipe (CFHP), the IFHP presents good fin temperature uniformity and heat performance; it eliminates the contact thermal resistance between the heat pipe and the heat sink, expands the condensation area of the heat pipe, and reduces the temperature difference between the fin base and the fin end. When the heat flux reached 161.1 W/cm^2, the fin efficiency increased to 93% and the temperature at the center of the evaporator bottom surface was merely 68.7 °C. For the IFHP, the optimal filling ratio and inclination angle are 30% and θ = 0°, respectively, for which the best heat performance was achieved, and the minimum total thermal resistance was 0.33 K/W. In the case of water cooling, the heat flux could reach up to 350 W/cm^2. The results indicate that the IFHP with copper foam as a porous network wick presents excellent heat performance, and is thus suitable for heat dissipation in high-heat-flux electronic devices.

1. Introduction

The thermal management of optoelectronic chips, such as the heat dissipation in high-power lasers, light-emitting diodes (LEDs), high-performance microprocessors, and infrared detector arrays, has become a sought-after research topic over the past few decades. Flat heat pipes, as two-phase heat transfer devices, offer a very promising solution. They hold the advantages of low heat transfer temperature difference, high heat transfer performance, small size, and excellent temperature uniformity [1–6].

Capillary wicks are core components that determine the heat performance of flat heat pipes through providing an extensive area with a thin evaporative film and pumping the working fluid from the condenser to the evaporator. Thus, numerous researchers have proposed various kinds of wicks to study the heat performance of flat heat pipes. According to the capillary wicks, the heat pipes are mainly classified into three types: (1) Groove wick heat pipes: Benson et al. [7] proposed silicon heat spreaders with wicks that were machined by using a dicing saw or the deep plasma etch process. The effective conductivity was more than five times that of silicon for a heat flux up to 15 W/cm^2. Hopkins et al. [8] investigated three kinds of axial-channel flat heat pipes, with a vapor channel cross-sectional area of approximately 1.5 × 12 mm^2 and rectangular grooves that were 0.20 mm wide by 0.42 mm deep. They found that the thermal resistance is a function of the evaporation and condensation area. The maximum heat flux on the evaporator wall exceeded 90 W/cm^2 in the horizontal orientation and 150 W/cm^2 in the vertical orientation. Using wires to fabricate grooves is a low-cost and simple method for mini heat pipes. A typical copper/water wire-plate mini heat pipe was investigated by Launay et al. [9], and the experimental results showed that its effective thermal conductivity was improved by a factor of 1.3 compared with that of the empty mini heat pipe array. Wang and Peterson [10] developed and designed a flat plate heat pipe by welding a sandwich of two flat plates with an array of parallel wires. They found that the maximum heat transport capacity increased with the increase in wire diameter and is proportional to the square of the wire diameter. An optimum design parameters existed at which the heat transports capacity reaches a maximum value. The optimum distance between two wires is approximately 2.5 times the wire diameter. Recently, Paiva and Mantelli [11]

* Corresponding author.
E-mail address: xjl@ncepu.edu.cn (J. Xu).

http://dx.doi.org/10.1016/j.expthermflusci.2017.03.008
0894-1777/

Nomenclature

A_{heat}	heater area, m^2
A_{eva}	evaporation area, m^2
CFHP	conventional flat heat pipe
d_e	effective pore diameter of the wick, m
h	heat transfer coefficient, $W/(m^2\ K)$
IFHP	integrated flat heat pipe
k	thermal conductivity, W/(m K)
L_f	fin height, m
L_p	cross section perimeter of the fin, m
$\dot{m}$	vapor mass flow rate, kg/s
ppi	number of pores per inch
Δp	capillary pressure, Pa
q	heat flux, W/cm^2
Q	heating power, W
R	thermal resistance, K/W
r	cylindrical coordinate, m
r_{lv}	latent heat of evaporation, kJ/kg
T	temperature, °C
dT/dx	temperature gradient
z	axial coordinate, m

Greek symbols

α	wetting angle, °
β	relative temperature uniformity coefficient
δ	wick thickness, m
ε	porosity
η	fin efficiency
φ	filling ratio
μ	viscosity coefficient, kg/(m s)
θ	inclination angle, °
ρ	density, kg/m^3
σ	surface tension, N/m

Subscripts

air	air
ave	average
c	center
e,sur	evaporator bottom surface
e	evaporator
e,c	evaporator bottom center
f	fin
fb	fin base
h	heat pipe
i,j,1–17	temperature measuring points
l	liquid
min	minimum
max	maximum
sat	saturation state
sur	surface
t	total
v	vapor
water	water

performed a theoretical thermal study on a wire-plate mini heat pipe. They developed a thermal model to predict the temperature distribution over the heat pipe surface and carried out some experiments to verify it. The results showed the developed thermal model was precise and that it could be used for the design of wire-plate mini heat pipes with high thermal performance. (2) Mesh wick heat pipes: Wang and Peterson [12] used sintered copper screen meshes as the primary wicking structure, in conjunction with a series of parallel wires, which formed liquid arteries. They found that the maximum heat transfer capability of heat pipes was affected by the mesh number, the wire diameter, the number of layers, the tilt angle, and the sintering process. For the plate heat pipe with six layers of 150 mesh screens, the heat flux could reach up to 19.1 W/cm^2. Liou et al. [13] visualized the evaporation characteristics in the evaporator of the heat pipe with different combinations of 100 and 200 mesh screens, and the wick thickness ranged from 0.26 mm to 0.8 mm. At various water charges, the evaporation resistances were measured and the evaporation behavior was visualized for heat fluxes of 16–100 W/cm^2. Quiescent surface evaporation without nucleate boiling was observed for all test conditions. With the increase in the heat flux, the water film receded and the evaporation resistance was reduced. The minimum evaporation resistance was found when a thin water film was sustained in the bottom mesh layer. (3) Sintered powder wick heat pipes: Xuan et al. [14] used sintered copper powder as a wick, and studied the performance and the mechanism of a flat heat pipe, finding that the porous sintered layer on the heated surface can enhance the evaporation process and the heat performance of the flat heat pipe. Such a technique ensured the proper operation of the heat pipe at a high heat flux in arbitrary orientation. Wong et al. [15] measured the evaporation resistances of loosely-sintered copper-powder evaporators in operating flat plate heat pipes. Uniform heating of 16–170 W/cm^2 was applied to the base plate near a pipe end with a heated surface of $1.1 \times 1.1\ cm^2$. The minimum evaporation resistance was approximately 0.08–0.09 $W\ cm^2/K$ for wicks containing fine powders.

In addition to the above types of heat pipes, Cai and Chen [16] designed and tested a heat pipe with carbon nanotubes as the wick. Owing to the high thermal conductivity of carbon nanotubes, the thermal conductivity of the heat pipe was improved significantly. To solve the conflict between vapor release and liquid suction, Chen et al. [17] investigated a miniature heat pipe with a biporous wick made of nickel powder. Tests demonstrated that the heat pipe could start at a heat load as low as 2.5 W. The maximum heat flux reached 12.8 W/cm^2 at the allowable evaporator temperature, which was below 60 °C. Huang and Franchi [18] concluded that the heat pipes with hybrid wick structures in various configurations could be four times higher in terms of effective thermal conductivity than those with only monolithic wick materials such as copper mesh. Sun and Qiu [19] proposed an asymmetric vapor chamber with micro/nanostructure. This kind of micro/nanostructure evaporator surface did not only improve the capillary capability of wick, but also provided more nucleation sites and expanded the heat transfer area. Therefore, the heat performance of the vapor chamber was improved.

Recently, the manufacturing technology of ultra-light porous metal foam has gradually matured. Being a novel multifunctional material, copper foam has high porosity, high thermal conductivity, and a large surface area, thus presenting high performance in the field of heat transfer [20]. Moreover, the use of metal foam for the wick is a simple and low-cost solution. Shirazy and Fréchette [21] studied the heat transfer limit of a flat heat pipe using metal foam as the wick. The results showed that a 60 ppi (number of pores per inch) has a higher boiling limit, approximately five times higher than that of the sintered metal powder wick. Ji et al. [22] designed a vapor chamber based on the copper

foam wick and found that the maximum heating power could reach 170 W, corresponding to a heat flux of 216 W/cm^2 without reaching capillary or boiling limits.

However, for the majority of heat pipe spreaders, the heat pipe and the heat sink are two separate devices that are assembled together to complete the heat dissipation process. Although thermal grease is used to ensure tight contact between the heat pipe and the heat sink, high contact thermal resistance is still present, which does not enable good heat dissipation. Moreover, a significant temperature difference exists between the fin base and the fin end, indicating that the fin efficiency is low. The high contact thermal resistance could be eliminated if the heat pipe and the heat sink became integrated; thus, fin efficiency could be greatly improved if the temperature difference between the fin base and the fin end was reduced. Based on the above reasons, there is a plethora of studies in the literatures dealing with the modeling and the optimization of heat sinks, which involved two types; that is conventional heat sink, such as in the work of Muzychka et al. [23], and the vapor chamber heat sink, such as in the work of Mochizuki et al. [24]. Recently Mantelli et al. [25] presented a new vapor chamber heat sink with maximum fin efficiency. The fins were hollow; therefore the vapor generated at the base can reach the top. As a result, the heat sink can be considered isothermal. The overall thermal resistance of the prototype was reduced by 20% compared with that of the conventional fin heat sinks with the same mass and volume. Furthermore, a theoretical model for the heat sink thermal resistance was developed, and the agreement between the model and the experimental data was fair.

In this study, we fabricated a novel IFHP with compressed copper foam as the porous network wick, which successfully solved the contact thermal resistance problem between the heat pipe and the fin heat sink. A layer of ultra-light porous copper foam was compressed and sintered on the inner surface of the evaporator as the capillary wick. Several channels were created in the fin heat sink, in which copper foam bars were inserted. Such a design did not only expand the condensation area, but also reduced the temperature difference between the fin base and the fin end, which greatly enhanced the heat performance of the IFHP.

2. Integrated flat heat pipe

Fig. 1 illustrates a schematic representation of the IFHP. It consists of a fin heat sink, copper foam bars, a sealing piece, a metal foam layer, a copper substrate (as the evaporator bottom plate), and a filling tube (Fig. 1(a). The fin heat sink was made from an aluminum cylinder, with 69 circular channels (holes) in it. At the bottom of the heat sink, there is a circular-straight groove network (Fig. 1(b)). Four straight channels cross at the center. The groove network can be used as a supporting structure and to connect all the channels, functioning as flow path that enables the distribution of vapor everywhere inside the heat pipe. A porous copper foam layer was sintered on the bottom copper plate as the evaporator wick (Fig. 1(c)). It has a thickness of 1.0 mm, which was compressed from a piece of copper foam of a 2.0 mm thickness. The copper plate has a thickness of 1.0 mm. To pump the liquid from the condenser to the evaporator, a copper foam bar was inserted into each of channels (holes), which made direct contact with the copper foam layer wick on the inner surface of the evaporator bottom plate. In order to achieve a vacuum environment and the need to inject the working liquid, a filling tube was connected to the evaporator.

Currently, electronic devices are designed to be both light weight and small. Therefore, in the present experiments, aluminum was used for the manufacturing of the heat pipe. Although the water has a high surface tension and a high latent heat of

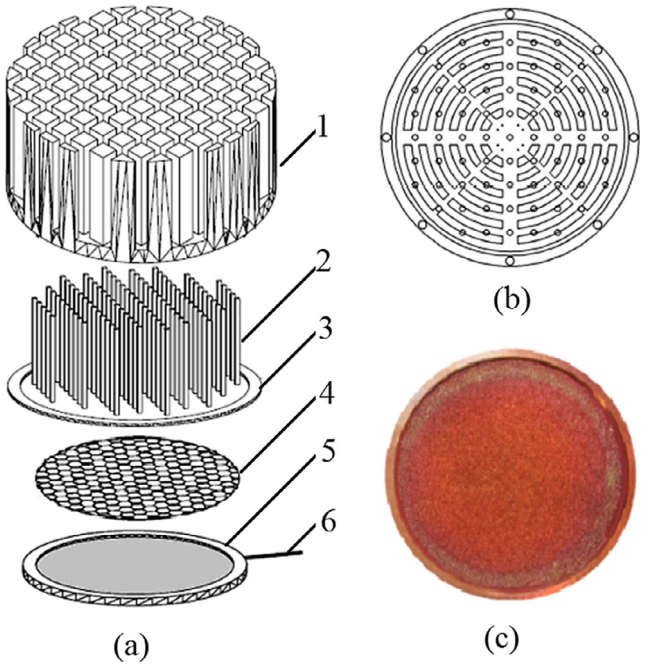

Fig. 1. Schematic representation of integrated flat heat pipe: (a) parts of the IFHP (1. heat sink; 2. copper foam bars; 3. sealing piece; 4. metal foam layer; 5. copper substrate; 6. filling tube); (b) bottom structure of fin heat sink; (c) copper foam layer wick sintered on the evaporator bottom plate.

vaporization in the given operating temperature range, the reaction of water/aluminum will generate hydrogen and other non-condensable gases, resulting in either high thermal resistance or complete malfunction of the heat pipe. Considering the compatibility of acetone/aluminum [26], acetone was used as the working fluid. The physical properties of acetone at the atmospheric pressure are listed in Table 1.

Fig. 2 presents the images obtained through scanning electron microscopy (SEM) of the copper foam used as the porous network wick. The SEM images show that the copper foam has a three-dimensional network structure, with random stochastic topology, where the metal skeleton branches overlap each other to form numerous interconnected cells; each cell has three to six holes of different shapes and sizes (diameter of ~0.5 mm) (Fig. 2 (a) and (c)). The high-porosity metal foam materials are purchased from Shanghai Abici Material Technology Co., Ltd., with a porosity of 0.95 and a ppi of 90. At present, the technology of preparing such high-porosity copper foam is mature, and it is achieved using electrochemical deposition [27]. In order to solve the problem of high porosity affecting the capillary force of the wick, the metal foam was compressed. Its porosity was reduced from 0.95 to 0.48. As seen from the compression direction, the aperture did not change and remained considerable in size (Fig. 2(b)), which is beneficial to the vapor release. As seen from a perspective perpendicular to the compression direction, the aperture has been greatly reduced (Fig. 2(d)) (diameter of ~0.08 mm). Hence, in the present work, we used compressed copper foam with a porosity of 0.48 instead of uncompressed copper foam of high porosity (i.e., 0.95), because the compressed copper foam can improve the capillary force of the wick. Hansen and Næss [28] used the compression method to obtain the desired capillary force for a nickel wick structure. Zhang et al. [29] experimentally verified that the compressed metal foam has multi-scale pores, resulting in the ability to pump a significant amount of liquid to a longer distance than a monoporous wick. In order to verify whether the porosity value of 0.95 or 0.48 is considered for the present work, we also performed a simple liquid

Table 1
Physical properties of acetone at the atmospheric pressure.

T_{sat} (°C)	ρ_l (kg/m^3)	r_{lv} (kJ/kg)	σ (N/m)	μ_l (Pa s)	k_l (W/m K)
56.29	761.18	512.94	0.0192	0.000237	0.518

Where T_{sat} is the saturation temperature, ρ_l is the liquid density, r_{lv} is the latent heat of evaporation, σ is the surface tension, μ_l is the liquid viscosity, and k_l is the thermal conductivity of liquid.

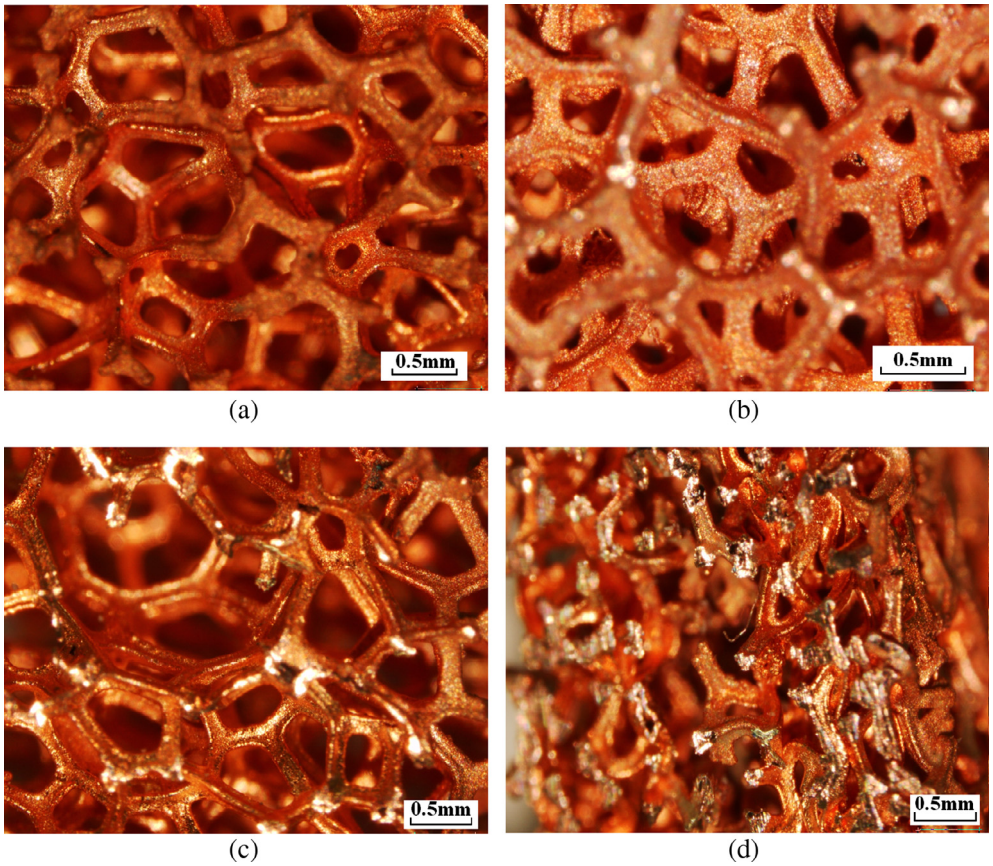

Fig. 2. SEM images of copper foam: (a) as seen from the compression direction before compression, (b) as seen from the compression direction after compression, (c) as seen from the perpendicular to the compression direction before compression, (d) as seen from the perpendicular to the compression direction after compression.

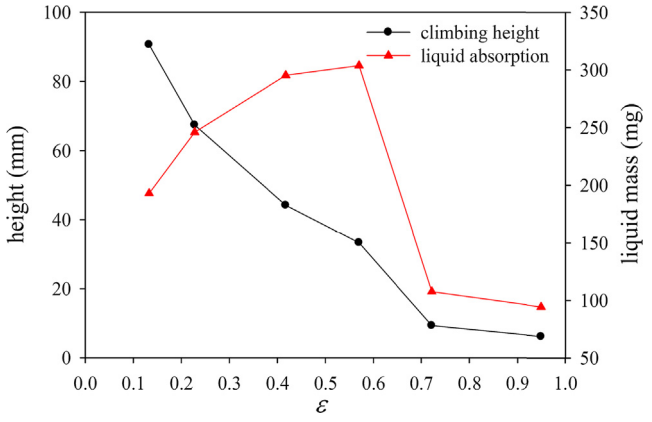

Fig. 3. Liquid climbing height and liquid absorption mass versus the porosity of the metal foam.

climbing experiment. Several samples with different porosity, which were made of uncompressed foam with different compression ratios, were tested. The climbing height and the liquid mass were recorded during a period of one minute (Fig. 3). The results show that the smaller the porosity, the higher the climbing height of the liquid. However, the metal foam with a porosity of 0.4–0.6 has a higher value than others for the amount of liquid absorption. When the porosity is high, both the climbing height and the amount of liquid absorption receive lower values. Furthermore, the heat pipe does not only need a significant capillary force for the liquid circulation, but also a great amount of liquid to meet the requirements of the phase-change heat transfer. Thus, based on the balance between the capillary force and the amount of liquid absorption, for the present work, the compressed metal foam with porosity value of 0.48, and not 0.95, was considered as the wicks. A systematic discussion of metal foams, used as wicks with and without compression, can be found in the literature [30].

The working principle of IFHP is significantly different from that of CFHP, as shown in Fig. 4. In the CFHP, the heat pipe and the heat sink are assembled together to enable heat dissipation (Fig. 4(a)). The temperature is uniform on the top surface of the flat heat pipe, however, it gradually decreased along the fins of heat sink; thus, a considerable temperature difference exists between the fin base and the fin end. Besides, the wicks of most CFHPs are distributed along the inner wall of the flat heat pipe, which increases the flow distance, the flow time, and the circulation resistance of the liquid.

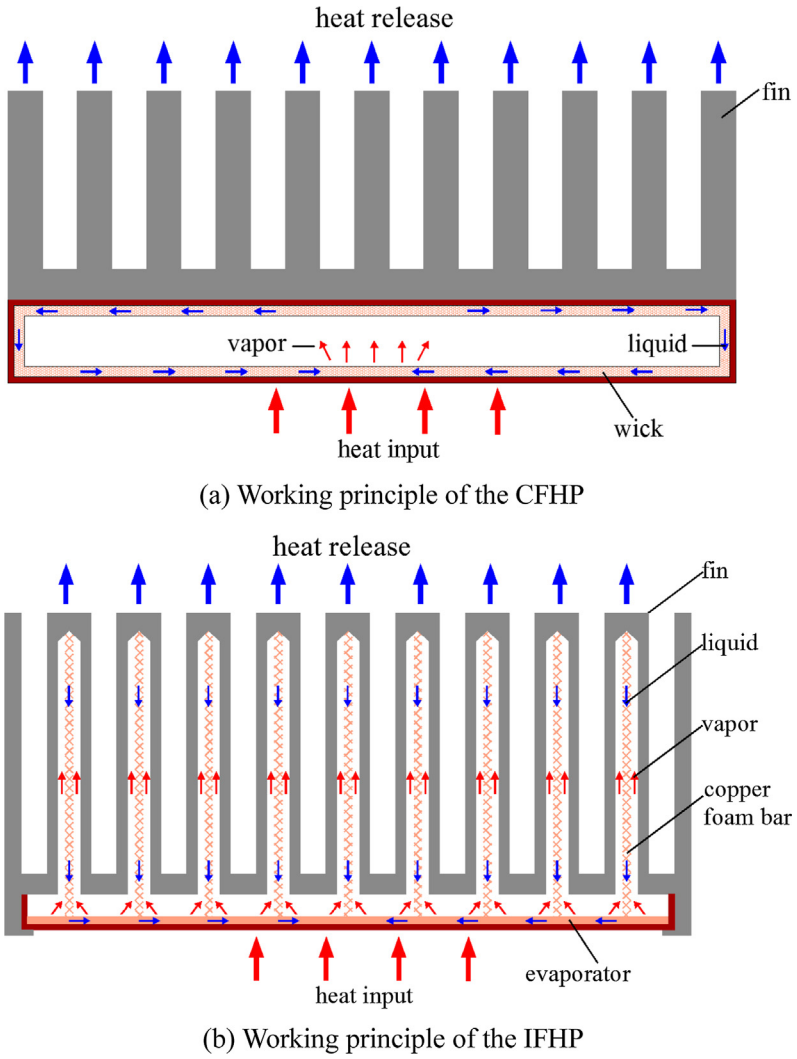

Fig. 4. Working principle of the CFHP and the IFHP.

However, in the IFHP (Fig. 4(b)), the heat pipe and the heat sink are integrated. When heated, the working fluid in the evaporator absorbs heat and transforms into vapor. Then, the vapor is freely distributed in the evaporation chamber and in the channels within the fins. Finally, the vapor is condensed and transformed into liquid. Owing to the capillary force, the liquid is sucked into the copper foam bars, and then flows into the evaporator wick, thus realizing the circulation of the working liquid. Therefore, each channel, in which a copper foam bar has been inserted, is similar to a miniature heat pipe after being coupled with other components. This means that there are several similar miniature heat pipes in the fin heat sink for the purpose of dissipating heat. By comparison, the IFHP has several advantages: (1) There is no contact thermal resistance between the heat pipe and the heat sink, which greatly contributes to the decrease in the thermal resistance of the whole heat spreader, particularly for the high heat-flux condition; (2) There is a small temperature difference between the fin base and the fin end; the fin efficiency has greatly improved along the fin height direction; (3) A larger condensation area is achieved by constructing channels within the fin heat sink; (4) The liquid flow path is shortened and the flow sectional area is increased for liquid returning to the phase-change heat transfer region; therefore, the liquid flow resistance is considerably lower than that of the conventional design, and the anti-dryout capability of the heat pipe was enhanced.

3. Experimental methods

3.1. Experimental setup

The experimental setup is shown in Fig. 5a. It mainly consists of a cooling system, a test section, a heating part, a data acquisition system, and a power supply unit. There are two types of cooling methods: air cooling and water cooling. For air cooling, a fan of 5 W was positioned on the top of the IFHP to cool the fin heat sink. Ambient temperature was approximately 25–27 °C. To study the effects of inclination angles on the heat performance, the test section was placed on a rotating plat form, and the inclination angles could accurately be adjusted. A copper block was used to heat the test section. A circular heating surface with a diameter of 10.0 mm was placed on the top end of the copper block, with a heating area of 0.785 cm^2. In the upper part of the copper block, there are three holes with a diameter of 1.0 mm, in which three K-type thermocouples (T_{15}–T_{17}) were inserted to measure the center temperature of the heating surface. At the bottom part of the copper block, there are five holes with a diameter of 8.0 mm, in which five 100.0 W cartridge heaters were inserted, providing heating power to the copper block. The five cartridge heaters were driven via a power supply unit consisting of a voltage stabilizer, an AC voltage transformer, and a power meter. By adjusting the voltage transformer, a stable voltage output could be obtained in the range of 0–

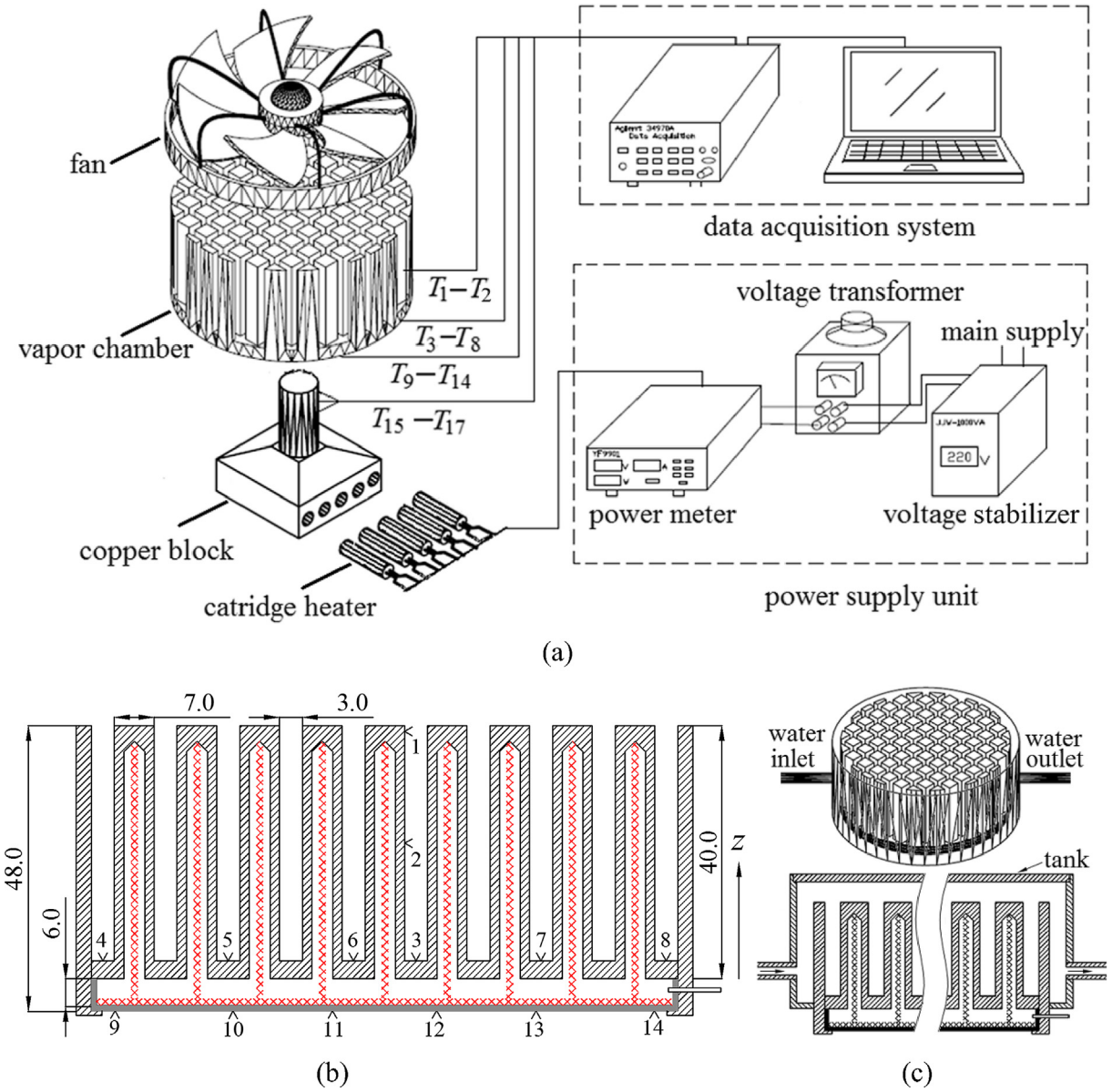

Fig. 5. Experimental setup: (a) configuration of test system, (b) section structure of IFHP and the distribution of temperature measuring points, (c) IFHP under the water cooling condition.

220 V, resulting in an adjustable heating power from 0 to 450.0 W. To reduce the contact resistance, the IFHP was welded on the heater surface using tin as a solder. A data acquisition system was used to record the temperature data and transfer them to the computer. To reduce the heat loss, heat insulating materials were used around the heating part.

Fig. 5(b) shows the section structure of the IFHP and the distribution of the temperature measuring points. The diameter and height of the whole IFHP are 100.0 mm and 48.0 mm, respectively. Except for two fins on both sides, each fin has a thickness of 7.0 mm and a height of 40.0 mm. The gap between two neighboring fin is 3.0 mm. The bottom thickness of the fin base is 6.0 mm and the diameter of each channel in the fin is 4.0 mm. The copper foam bar inserted in the hole has a square cross section with a side of 1.5 mm. Except for T_{15}–T_{17} introduced above, T_{18} is designated for the measurement of the ambient temperature. There are fourteen K-type thermocouples to measure the temperature distribution on the surface of the IFHP. Among them, T_1–T_2 measure the temperature distribution along the direction of the fin height; T_3–T_8 were welded on the fin base surface, and the arithmetic mean of the six measured temperatures yields the average temperature of the fin base. Thermocouple T_3 is located below T_1 and T_2; therefore T_1–T_3 can be used to calculate the fin efficiency. Finally, T_9–T_{14} were welded on the evaporator bottom surface to specify the temperature distribution of the evaporator bottom surface.

Under the water cooling condition, the IFHP was embedded in a circular water tank (Fig. 5(c)). The figure illustrates a tank (actually opaque), so that the fin heat sink in the tank can be seen. Across section of the configuration is also shown in Fig. 5(c). Cooling water flows into the tank from one side and then flows out from the other side after exchanging heat with heat sink. The temperature of the cooling water was maintained at 25 °C at the inlet. A set of K-type thermocouples were placed at the selected locations on the fin base, the fin, and the evaporator bottom surface of the IFHP, in a similar manner to the distribution of the temperature measuring points under the air cooling condition.

Whether the air cooling or water cooling method is followed, their similarity pertains to the use of the forced convective heat transfer mode to cool the fins of the IFHP. Their difference mainly lies in two aspects. (1) The cycle mode is different. For the air cooling method, a fan was used to force the air to flow. The air entered from the fin end and would exit from around the heat sink. However, for the water cooling method, a pump was used to force the water to flow. The water flowed into the tank from one side, and exited from another side. (2) The cooling capacity is different. Compared with the air cooling method, the water cooling has a greater cooling capacity. In the present experiments, the purpose of the comparison between the two cooling methods is to investigate the effects of the cooling capacity of the external environment on the heat performance of the IFHP, because the water cooling method is often used to cool the heat sink or the condensation end of the heat pipe in certain high heat flux fields [31].

The experiments presented in this study were conducted at different inclination angles, which mainly aim to assess the anti-gravity performance of the IFHP in relation to the flow of the working fluid inside the heat pipe, and not to the cooling methods. The inclination angles of the IFHP are $\theta = 0°$, 90°, and 180°, where $\theta = 0°$ or 180° refers to the evaporator below or above the condenser. At $\theta = 180°$, the liquid in the IFHP has to overcome gravity to flow from the condenser to the evaporator. Nevertheless, gravity may enable the liquid to flow at $\theta = 0°$.

3.2. Experimental method and analysis

To reduce the contact resistance, the copper foam layer needed to be sintered on the inner surface of the evaporator bottom plate to form the evaporator wick. Before sintering, the copper foam layer and the bottom plate were successively cleaned using acetone and distilled water. Then, a small amount of copper powder with a particle diameter of 88 μm was spread on the evaporator bottom plate, forming a powder layer with a thickness of 0.1 mm. Finally, the copper foam layer was pressed on the copper powder with a certain pressure, and next they were sent into the furnace for sintering. The sintering temperature was maintained at 850 °C for 3 h, using hydrogen/nitrogen gas for protection from oxidation. The copper foam bars inserted into the channels could be obtained by cutting the compressed metal foam pieces. The length of the copper foam bars needed to be slightly longer than the actual demand to ensure close contact with the evaporator wick. After the copper foam bar had been inserted into each of the channels, the evaporator bottom plate with the porous wick covered the heat sink. The raised edge of the evaporator bottom plate was contact with the bottom edge of heat sink (see Fig. 4 (b)). Therefore, copper foam bars directly contacted the evaporator wick, and thus the porous network wick was formed. Finally, a copper-aluminum welding wire was used for the peripheral welding of both the copper plate and the heat sink base, so that the heat sink and the copper plate are welded together. After the assembly of the IFHP, air was injected with a pressure of 0.2 MPa. Then, the IFHP was placed into soapy water for leak detection. If no bubbles emerge, the heat pipe does not have any leakages and is packaged well. Finally, a vacuum pump was used to pump the IFHP for 15 min, while it was being heated. When the pressure reached 6×10^{-4} Pa, acetone was injected into the IFHP, and then the filling tube was sealed. Thus, the preparation of the IFHP was completed, and it could be used for experiments.

In this study, the flow of working liquid in the flat heat pipe is a vapor-liquid two-phase flow. The total circulation of the working fluid includes the evaporation of the liquid, the flow, as well as the condensation of the vapor and the flow of the liquid. Therefore, the relationship between vapor release and liquid supply needed to be optimized correctly. Considering the vapor release, Meléndez and Reyes [32] expressed the vapor mass flow rate in porous media as:

$$\dot{m} = \frac{\pi}{128}\left(\frac{\rho_v \sigma}{\mu_v}\right)\left(\frac{\varepsilon d_e^3}{\delta}\right) \tag{1}$$

where ρ_v, μ_v, σ, and ε are the vapor density, the viscosity, the surface tension, and the porosity respectively; δ is the wick thickness; d_e is the effective pore diameter. It can be seen from Eq. (1) that a higher vapor mass flow rate requires a larger pore size. However, the liquid supply is related to the capillary pressure as in the following:

$$\Delta p = \frac{4\sigma}{d_e}\cos\alpha \tag{2}$$

where α is the contact angle. A small pore size is needed to create sufficient capillary pressure for liquid circulation. The above analysis indicates that the liquid supply and the vapor release require different pore sizes. Hence, the copper foam was compressed to meet the demands of liquid supply by reducing the pore sizes and maintaining the pore sizes constant in the direction of the vapor release. Certainly, compressing the metal foam comes with the cost of decreasing the porosity and reducing the mass flow rate. However, as seen in Fig. 2, the pore diameter of the metal foam was significantly reduced by compression. This reduction of the effective pore diameter is more significant than the consequences of the accompanying decrease in porosity.

Because the copper block under the flat heat pipe was wrapped with heat insulation materials, the heat conduction process in the copper block can be treated as one-dimensional unsteady heat conduction. The center temperature of the evaporator bottom surface $T_{e,c}$ can be decided in terms of a linear relationship between T_{15}, T_{16}, and T_{17} (see Fig. 5a). The heat flux is

$$q = \frac{Q}{A_{heat}} \tag{3}$$

where Q is the heat load, and A_{heat} is the heating area. The total thermal resistance R_t, the fin resistance R_f, and the heat pipe resistance R_h are defined, respectively, as:

$$R_t = \frac{T_{e,c} - T_{air}}{Q} \tag{4}$$

$$R_f = \frac{T_{fb,ave} - T_{air}}{Q} \tag{5}$$

$$R_h = \frac{T_{e,c} - T_{fb,ave}}{Q} \tag{6}$$

where T_{air} is the ambient temperature, $T_{e,c}$ is the center temperature of the evaporator bottom plate surface, and $T_{fb,ave}$ is the average temperature of the fin base surface. Under the water cooling condition, T_{air} should be replaced by T_{water} in Eqs. (4) and (5).

The fin efficiency characterizes the heat performance of the fin heat sink, which is defined as the real dissipated heating power divided by that assuming a uniform temperature along the fin height with the temperature at the fin base:

$$\eta = \frac{\int_0^{L_f} h(T - T_{air})L_p dL}{h(T_3 - T_{air})L_p L_f} \approx \frac{\frac{1}{3}\sum_{i=1}^{3} T_i - T_{air}}{T_3 - T_{air}} \tag{7}$$

where h is the air convective heat transfer coefficient, T_i (i = 1, 2, 3, the thermocouple points) is the fin temperature (see Fig. 5(b)), L_f is the fin height, and L_p is the cross-section perimeter of the fin.

In order to characterize the uniformity of the temperature distribution on the fin base surface and the evaporator bottom surface of the flat heat pipe, we defined a new parameter, namely a relative

temperature uniformity coefficient (β) for the fin base surface and the evaporator bottom surface, respectively:

$$\beta_{fb} = \frac{T_{fb,\max} - T_{fb,\min}}{T_{fb,\max}} \quad (8)$$

$$\beta_{e,sur} = \frac{T_{e,\max} - T_{e,\min}}{T_{e,\max}} \quad (9)$$

where $T_{\mathrm{fb,max}} = \max\{T_3–T_8\}$, $T_{\mathrm{fb,min}} = \min\{T_3–T_8\}$, $T_{\mathrm{e,max}} = \max\{T_9–T_{14}\}$, and $T_{\mathrm{e,min}} = \min\{T_9–T_{14}\}$.

In the present experiments, the temperature measurement has a maximum uncertainty of 0.3 °C, and the heat load measurement has a relative error of 0.5%. Thus, the uncertainty of the thermal resistance was less than 6.4%.

4. Results and discussion

4.1. Validation and comparison

As the structure of our integrated heat pipe is different from the ones in the literature, and as the size of the heating area, working fluid, cooling intensity, and cooling area of the heat sink can all influence the thermal resistance, it is difficult to find an appropriate comparison with other published results. To validate the experimental results of the novel design used in this study, we first compared the thermal resistances of the CFHP (Fig. 4(a)) with that of vapor chamber studied by Ji et al. [22], as they have similar dimensions and test conditions, the same working fluid, and use metal foam as capillary wicks. A reasonable agreement between CFHP and the literature data was observed in Fig. 6: their thermal resistance values are close to each other for the same heat flux except some data points in the high heat flux region. Therefore, our measurement and calculating method are determined to be reliable. We also validated the experimental data of IFHP (Fig. 4 (b)) with that of Go [33] and Hsieh et al. [34]. Their thermal resistance values and range of the heat flux are different due to different wick structure and heating area, but the trends observed with increasing heat flux are the same. This indicates that the experimental values of the IFHP are reasonable in the regulation that thermal resistance changes with the heat flux.

Besides, the condenser of IFHP being composed of several hollow fins that is identical to the condenser of a two-phase thermosyphon. Kaminaga et al. [35] showed that the condensation resistance represents only 3% of the total resistance of heat pipe. This is due to the condensation area being much larger than the boiling area, and the condensation heat transfer coefficient being larger than the boiling coefficient, as the condensation heat transfer belongs to film condensation [36]. Therefore, the evaporation/boiling resistance controls the thermal resistance of IFHP at $\theta = 0°$. In this case, the heat pipe resistance is approximately equal to the evaporation/boiling resistance, $R_h = 1/hA_{eva}$. However, for the CFHP, the condensation resistance is not neglected. Thus, when two heat pipes function properly, the IFHP should have a smaller thermal resistance than the CFHP. Considering that nucleate boiling prevails at the evaporator of the IFHP, the thermal resistance due to the boiling at the evaporator can be expressed by the correlation of Forster and Zuber [37]. As shown in Fig. 6, except for $q < 16$ W/cm^2, a good agreement between the theoretical values and the experimental results for the IFHP was achieved, especially for $q > 34$ W/cm^2.

4.2. The effects of filling ratios

The filling ratio (φ) is defined as the liquid volume divided by the total inside volume, which is an important parameter of the heat pipe. Based on our previous study [22], the suitable filling ratio lies within the range of 10–40%, therefore, filling ratios of 15%, 20%, 30%, and 40% were performed in this study. Fig. 7 shows the effects of the filling ratios on the heat performance of the IFHP under air cooling condition. For each filling ratio, $T_{e,c}$ increases with the increase in the heat flux. Among four filling ratios, the IFHP with a filling ratio of 15% presents the highest $T_{e,c}$ for the same heat flux. When the filling ratios are lower than 30%, $T_{e,c}$ gradually decreases with the increase in the filling ratios for the same heat flux. However, when the filling ratios are over 30%, up to 40%, $T_{e,c}$ does not further decrease. In Fig. 7, there are two curves of $T_{e,c}$ versus the heat flux that are close to each other for $\varphi = 20\%$ and 40%; their respective $T_{e,c}$ values are approximately equal to each other for the same heat flux. These results show that the optimal filling ratio is 30% for the IFHP. The reason is that the filling ratio of 15% would be too low at an increasing heat load; the evaporation region would lack liquid supply and could easily dryout, leading to a high $T_{e,c}$. When the filling ratios exceed a certain value, a certain amount of liquid will accumulate in the evaporator, which would block the vapor channel and increase the resistance of vapor

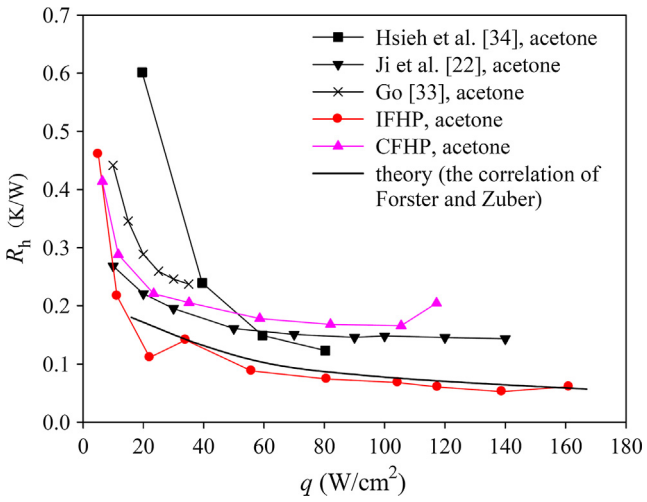

Fig. 6. Comparisons of thermal resistances among the present study, those reported in the literature, and the theoretical values.

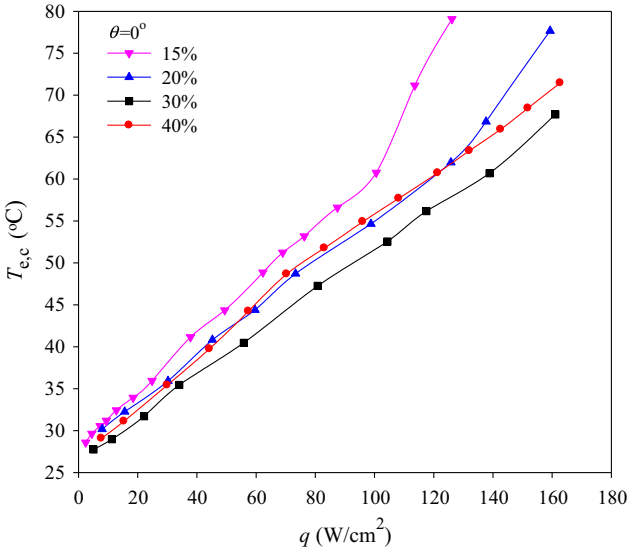

Fig. 7. Effects of the filling ratios on the center temperature of the evaporator bottom surface.

release. Therefore, there is a need to determine the optimal filling ratio.

4.3. Temperature uniformity

Fig. 8 shows the temperature distributions on the fin base surface and the evaporator bottom plate surface at $\theta = 0°$. The horizontal coordinator represents the distance of the temperature measuring point from the center point. The CFHP and the heat sink have the exact same bottom surface size, and the fins used for heat dissipation are the same material as in the IFHP. As shown in Fig. 8 (a), the fin base surface of the IFHP presents highly uniform temperature distributions for three different heat flux values (measuring points T_3–T_8 in Fig. 5(b)). The lower the heat flux, the better the temperature uniformity. At $q = 161.1$ W/cm^2, the maximum temperature does not exceed 64.8 °C, and the maximum temperature difference is less than 2.7 °C between six temperature values. Fig. 8(b) presents the temperature uniformity of the evaporator bottom plate surface of the IFHP (measuring points T_9–T_{14} in Fig. 5(b)). The temperature is high at the center zone and decreases with the increase in the distance away from the center point. Fig. 8 (c) shows the comparison of the temperature distributions on the fin base surface for the heat sink, the CFHP, and the IFHP. For the IFHP, the highest temperature and the maximum temperature difference between the measuring points on the fin base surface is 53.9 °C and 1.6 °C at $q = 117.2$ W/cm^2, respectively. However, for the CFHP and the heat sink, the highest temperatures are 55.4 °C and 60.5 °C, and the maximum temperature difference is 2.4 °C and 7.7 °C, respectively. It is apparent that the IFHP presents the lowest temperature and the best temperature uniformity on the fin base surface among the three heat spreaders, when their bottom plates are heated with the same heat flux. On the evaporator bottom plate surface, the advantage of the IFHP is more obvious (see Fig. 8(d)). Regarding the IFHP, the highest $T_{e,sur}$ is 56.2 °C, and the maximum temperature difference is 7.3 °C at $q = 117.2$ W/cm^2. For the heat sink, however, the highest $T_{e,sur}$ is 83.2 °C, and the maximum temperature difference reaches 26.8 °C. The reason why the IFHP has the best temperature uniformity and the lowest temperature is that 69 channels have been machined in the fins, in which copper foam bars were inserted, and are similar to 69 miniature heat pipes operating simultaneously. Among the three heat spreaders, the IFHP is the optimal solution to be applied for the heat dissipation of high-power and high-flux electronic devices.

To study how the temperature uniformity varies with the heat flux on the fin base surface and the evaporator bottom plate surface of the IFHP, the relative temperature uniformity coefficients versus the heat flux are illustrated in Fig. 9. Regarding the evaporator bottom plate surface, the uniformity coefficient ($\beta_{e,sur}$) increases with the increase in the heat flux, for $q < 117$ W/cm^2. However, $\beta_{e,sur}$ begins to decrease when the heat flux exceeds 117 W/cm^2. For the fin base surface, the uniformity coefficient (β_{fb}) has a similar regularity to $\beta_{e,sur}$, however, β_{fb} is lower than $\beta_{e,sur}$. When the heat flux reaches 117 W/cm^2, β reaches a maximum value of approximately 0.17 for the evaporator bottom plate surface and 0.09 for the fin base surface. This phenomenon can be explained by the following reasons. If no phase-change heat transfer takes place on the inner surface of evaporator, according to the Fourier Formula $q = -kdT/dx$ (k is the thermal conductivity of solid copper, dT/dx is the temperature gradient), the relationship between the temperature gradient and the heat flux is nearly linear from the center to the edge of the evaporator bottom plate; hence, $\beta_{e,sur}$ should linearly increase with the increase in heat flux. However, owing to the existence of phase-change heat transfer, which increases with the increase in q, $\beta_{e,sur}$ nonlinearly increases with the increase in q, and the slope of curve gradually decreases. Once

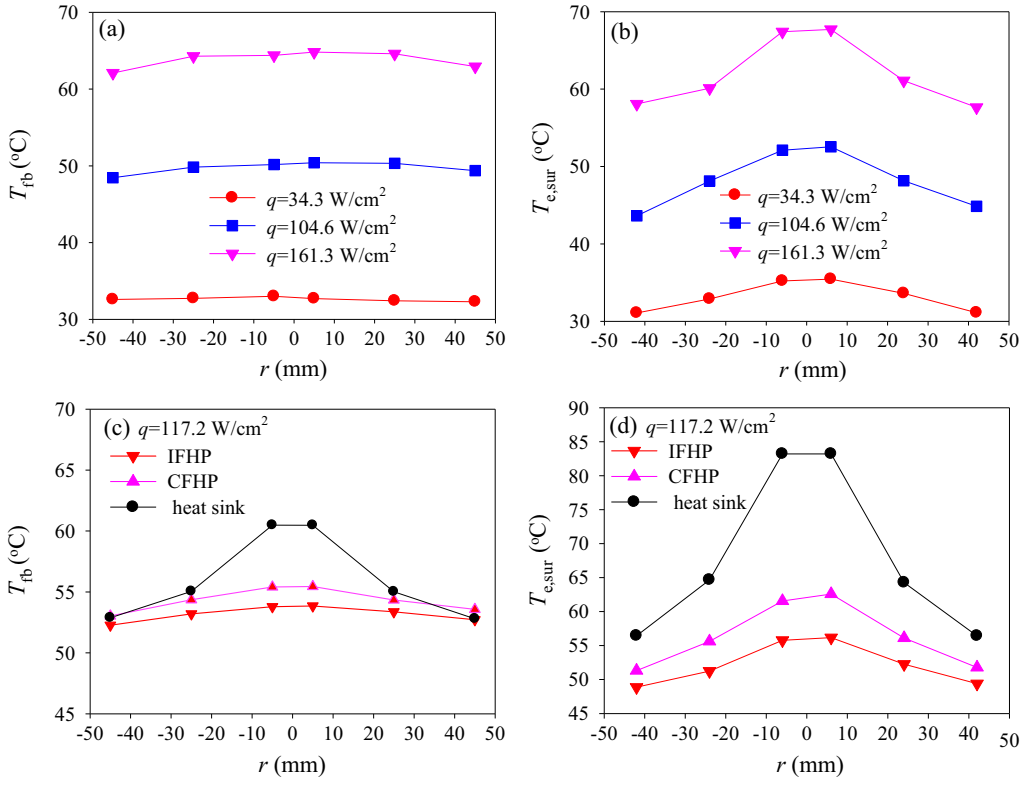

Fig. 8. Temperature distribution: (a) and (c) are the temperature distributions on the fin base surface, (b) and (d) are the temperature distributions on the bottom surface of three heat spreaders.

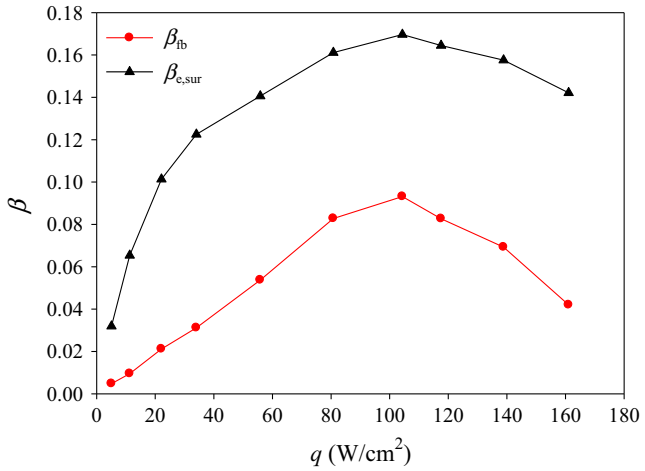

Fig. 9. Relative temperature uniformity coefficient β versus heat flux.

phase-change heat transfer region begins to expand from heating region, $\beta_{e,sur}$ reaches the maximum value. When the heat flux further increases, the phase change heat transfer also occurs on the non-heating region near the heating region, $\beta_{e,sur}$ begins to decrease with the increase in q. For the fin base surface, the condensation of vapor mainly occurs at the central region of the top surface of the heat pipe for a low heat flux and $\theta = 0°$; therefore, the temperature at the central region is high, and it increases with the increase in q, thus, β_{fb} gradually increases. When the vapor condensation area begins to expand from the central region, the maximum β_{fb} is achieved. After that, β_{fb} decreases with the increase in q. When the vapor is condensed throughout the top surface of the heat pipe, the whole of the fin base presents good uniformity at a high heat flux.

4.4. Fin efficiency

Fig. 10(a) shows the relationship between fin temperature T_f and fin height z at $\theta = 0°$. Compared with the CFHP and the heat sink, the IFHP significantly improves the temperature uniformity along the fin height. Regarding the CFHP and the heat sink, the temperature difference between the fin base and the fin end is approximately 14.7 °C and 21.9 °C, respectively, at $q = 161.1$ W/cm^2. However, for the IFHP, the temperature difference is approximately 7.1 °C; this is lower by 7.6 °C and 14.8 °C than that of the CFHP and the heat sink, respectively. Moreover, the temperature of the IFHP is lower than that of the CFHP and the heat sink on the fin base surface, which is most obvious at a high heat flux. Fig. 10(b) shows the fin efficiency (η) of the three heat spreaders for different heat fluxes. Regarding heat sink, if the heat flux is less than 34.4 W/cm^2, η increases with the increase in the heat flux. If the heat flux exceeds 34.4 W/cm^2, then η almost ceases to increase, and its maximum value is approximately 78%. For the CFHP, its turning point is at 56.1 W/cm^2, and following that, η has nearly reached a steady state and has a maximum value of 82%. However, there is a great difference for the IFHP; η continues to increase with the increase in heat flux until the heat flux exceeds 104.4 W/cm^2. The maximum value of η reaches 93% at $q = 161.1$ W/cm^2, which is the highest among the three heat spreaders. The reasons for this are as follows. The vapor is the heat carrier and can flow quickly along the channels in the fins of the IFHP; thus, the heat is transferred directly to the fin end and the thermal resistance is low. However, the fins of the CFHP and the heat sink are solid; therefore, the heat is transferred from fin base to the fin end through conduction, and the thermal resistance is high. Thus, the IFHP presents a smaller temperature difference between the fin base and the fin end compared to that of the CFHP and the heat sink. According to Eq. (7), for the same heat flux, the smaller the temperature difference between the fin base and the fin end, the higher the fin efficiency. Therefore, the IFHP presents the highest η among the three heat spreaders. Owing to its novel design, the IFHP has 69 similar miniature heat pipes that simultaneously take part in the heat transfer, which significantly enhances the temperature uniformity of the whole fin heat sink. As a result, the heat performance is enhanced and the temperature of the fin base decreased. This is the reason why the temperature of the IFHP is lower on the fin base surface than that of the CFHP and the heat sink. Still, the question arises as to why the fin efficiency is lower for low values of heat flux in the present experiments. According to the literature [38], η increases with the increase in the thermal conductivity of the fins, and decreases with the increase in the convective heat transfer intensity. On the one hand, the thermal conductivity of aluminum increases with the increase in temperature within the range of 0–100 °C. The temperature of the fins is low at low heat flux values; hence, the thermal conductivity and η are both low. On the other hand, the temperature of the air in the gaps between the fins increases with the increase in heat flux, not only contributing to the decrease in the convective heat transfer, but also leading to increased buoyancy. Large buoyancy would follow the direction opposite to that of the air flow driven by the fan, and would decrease the convective heat transfer coefficient on the fin surface. Therefore, the convective heat transfer intensity is higher and the corresponding η is smaller at a low heat flux than those at a high

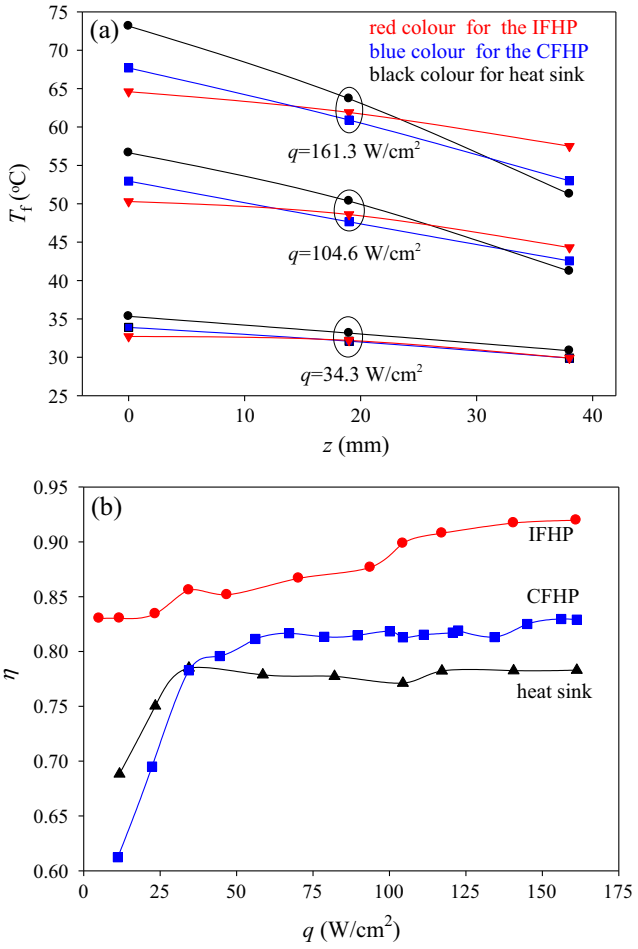

Fig. 10. Temperature distribution on the fin surface (a), and fin efficiencies versus the heat flux (b).

heat flux. When the temperature reaches a certain value, the effects of various factors tend to stabilize, and η reaches its maximum value at a high heat flux. Although both the CFHP and the heat sink have solid fins, the temperature of the fin base is uniform and lower for the CFHP compared with that of the heat sink, for the same heat flux (see Fig. 10(b)). Hence, the CFHP requires significant heat flux to reach the turning point where the convective heat transfer intensity tends to weaken.

Regarding the heat sink and the CFHP, the fin efficiency decreases with the increase in fin height, therefore, the fin height is limited to certain values. However, for our novel design, it is viable to make the fin height higher than that of the heat sink because the vapor can directly arrive at the fin end through the channels in the fins, and the temperature difference between the fin base and the fin end is small.

4.5. Effects of inclination angles and cooling methods

The relationship between gravity and the flow direction of the working fluid significantly affects the vapor-liquid distribution and flow, and further affects the heat performance of the heat pipe. Thus, it is necessary to study the effects of the inclination angles. Fig. 11(a) shows that $T_{e,c}$ varies with the heat flux, at different inclination angles. For the three heat spreaders, $T_{e,c}$ increases with the increase in the heat flux at $\theta = 0°$, 90°, and 180°. For the same heat flux, e.g., $q = 90$ W/cm^2, the $T_{e,c}$ of the IFHP is lower than that of the heat sink and the CFHP at $\theta = 0°$. For the CFHP and the IFHP, the temperature inside the heat pipe was maintained less than 80 °C. If the temperature exceeded 80 °C, the pressure inside the heat pipe would have been higher than 224 kPa, and the internal pressure would have been greater than the external environmental pressure (101 kPa); this would cause the deformation of the evaporator bottom plate. The relationship between the temperature and the saturation pressure is listed in Table 2. For the same $T_{e,c}$, e.g., $T_{e,c} = 80$ °C, the IFHP can expand the range of heat fluxes to an upper limit of 161.1 W/cm^2, whereas that of the CFHP is 117.2 W/cm^2. Furthermore, Fig. 11(a) illustrates that the $T_{e,c}$ values of the IFHP and the CFHP are lower at $\theta = 0°$ than those at $\theta = 180°$; this occurs because gravity can help the liquid to flow from the condenser to the evaporator at $\theta = 0°$. On the contrary, gravity significantly impedes the movement of the fluid at $\theta = 180°$, thus affecting the liquid supply.

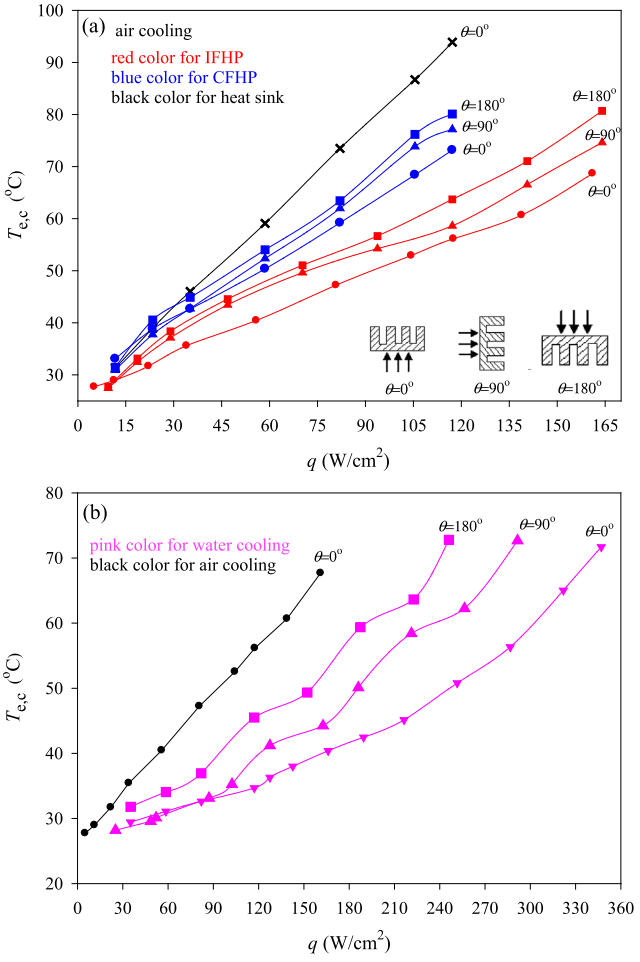

Fig. 11. Center temperatures of evaporator bottom plate surface versus heat flux for different inclination angles.

Many factors can affect the heat performance of the heat pipe during the operation. One of them is the cooling method, which plays a very important role in the heat transfer of the heat pipe. Therefore, both air and water cooling methods were implemented to study their effects on the IFHP. Under water cooling conditions, the effects of the inclination angles and the change trend of $T_{e,c}$ with increasing heat flux were similar to those occurring under air cooling conditions (Fig. 11(b)). However, $T_{e,c}$ considerably decreased, when the heat flux reached 160 W/cm^2 at $\theta = 0°$, and $T_{e,c}$ was 25 °C less than that under air cooling conditions. When the heat flux reached approximately 350 W/cm^2, the $T_{e,c}$ was only 72 °C. It can be observed that water cooling can rendered the IFHP efficient at higher heat flux than air cooling for the same $T_{e,c}$. These results reveal that the IFHP is suitable for heat dissipation in high-heat-flux electronic devices, and water cooling can be used to replace air cooling when the heat flux is high.

4.6. Analysis of thermal resistance

Fig. 12(a) shows that for all three heat spreaders, the total thermal resistance R_t varies with increasing heat flux under air cooling conditions at $\theta = 0°$. Regarding the heat sink, the total thermal resistance R_t remains at the same value of approximately 0.75 K/W versus the heat flux. When the heat flux exceeds 23.4 W/cm^2, the heat sink has the highest value of R_t among the three heat spreaders. However, the IFHP has the lowest R_t and the CFHP has an in-between thermal resistance value. Regarding the CFHP, the minimum value of R_t is 0.52 K/W, whereas that of the IFHP is only 0.32 K/W. For the IFHP and the CFHP, R_t is lower at $\theta = 0°$ than at $\theta = 180°$. Under water cooling conditions, the R_t of the IFHP is significantly lower than under air cooling conditions, regardless of the inclination angle ($\theta = 0°$ or 180°). The best thermal performance can be achieved, and the minimum R_t is 0.12 K/W at $\theta = 0°$ and $q = 117.2$ W/cm^2. Moreover, in the case of water cooling, the IFHP can operate within a wide range of heat fluxes and up to 350 W/cm^2, thus presenting excellent heat performance.

More specifically, R_t consists of R_h and R_f. Fig. 12(b) shows the relationship of R_t, R_h, and R_f for the IFHP. At a low heat flux ($q < 11.3$ W/cm^2) R_t and R_h are higher than R_f; R_t is mainly affected by R_h. Regarding R_f, it is affected by the thermal conductivity of the fins and the external environment. Owing to the combination of the driving force by a fan and the buoyancy force affected by the air temperature between the fin gaps, the convective heat transfer coefficient on the fin surface is high at low heat fluxes, and does not relate to the heat flux at high heat fluxes; therefore, R_f receives low values at low heat fluxes, and maintains a steady value at high heat fluxes. However, before the IFHP starts up, the R_h is mostly affected by the heat conduction and the convective heat transfer in the evaporator; the thermal resistance is relatively high. After the IFHP starts up, the R_h is mostly affected by the phase-change heat transfer, and the thermal resistance is low; hence, R_h

Table 2
Relationship between temperature and saturation pressure.

Temperature (°C)	0	20	40	60	80	100	120	140
Saturation pressure (kPa)	8.9	24.6	56.2	116	224	372	608	945

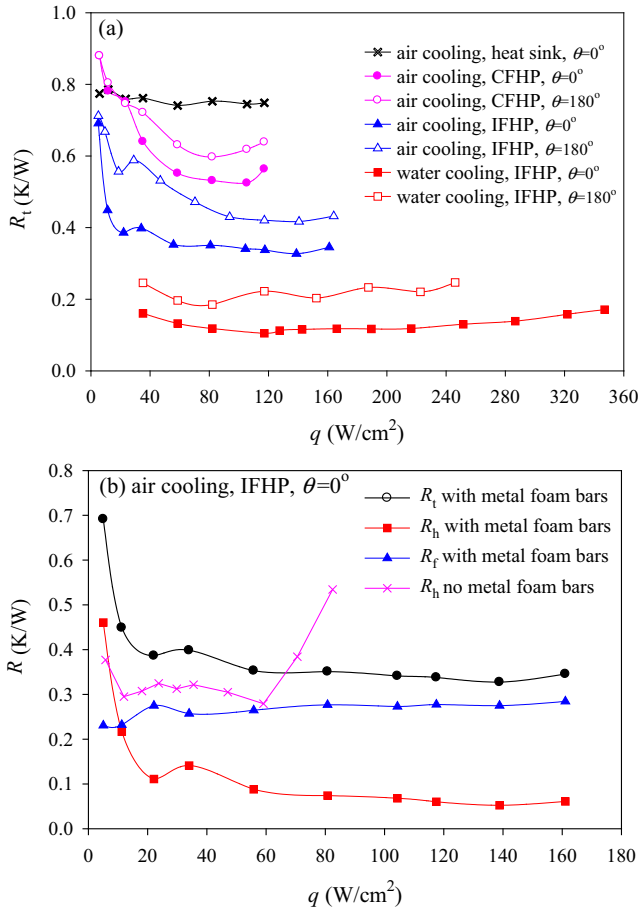

Fig. 12. Thermal resistance versus heat flux.

decreases with the increase in heat flux until reaching a steady value. This is also the reason why the heat pipe should present good sealing performance. It is obvious that R_h is low for our novel design. Our next step will be to optimize the fin structure to further reduce the overall thermal resistance.

In the cases where $\theta = 180°$, the metal foam bars are required to be inserted into the channels of the IFHP to carry the liquid from the condenser to the evaporator. At $\theta = 0°$, are metal foam bars needed to insert into the channels? Owing to the effects of surface tension and vapor pressure in the evaporator, if the diameter of a channel is small and the liquid wets the channel walls, the liquid cannot flow out from the channel once the channel has been fully filled with condensed liquid; although the gravity can help liquid to flow. This is similar to the example of a glass tube with a small inner diameter, which is fully filled with water; the water cannot flow out if the tube is turned upside-down. The pink curve in Fig. 12(b) shows the heat performance of the IFHP without metal foam bars inserted into the channels; its R_h value is higher than that of the IFHP with metal foam bars. When the heat flux reaches 60 W/cm^2 at $\theta = 0°$, R_h sharply increases, indicating that the IFHP without metal foam bars has reached the heat transfer limit.

To summarize, the exceptional heat performance of the IFHP can be explained as follows: (1) The porous copper foam has a high thermal conductivity, which is helps to improve the effective solid-liquid heat transfer coefficient, contributing to the enhancement of the heat transfer capability. (2) After the copper foam was compressed, there were numerous small and large pores in the copper foam wicks. Large pores can reduce the flow resistance of the working fluid, and small pores can provide high capillary pressure to enhance liquid supply. Thus, the existence of small and large pores has a synergetic effect, which enables the copper foam wick to achieve the best heat performance. (3) The IFHP realizes the integration of the fin heat sink with the heat pipe, which can eliminate the contact thermal resistance between them. Meanwhile, the IFHP expands the heat transfer area of the condenser, which helps heat dissipation. Furthermore, 69 channels were machined in the fins, in which copper foam bars were inserted; these channels coupled with wicks are equivalent to 69 miniature heat pipes that operate simultaneously.

5. Conclusions

A novel IFHP was fabricated, with compressed copper foam as porous network wick. Experiments were conducted to investigate the effects of filling ratios, cooling methods, heating power, and different inclination angles on its heat performance. The conclusions can be summarized as follows:

- The novel IFHP presented better temperature uniformity and the stronger heat dissipation ability compared with the heat sink and the CFHP, under the same experimental conditions. The contact thermal resistance between the heat pipe and the heat sink was eliminated, the condensation area of the heat pipe was expanded, and the temperature difference between fin base and fin end was reduced. Thus, fin efficiency was enhanced and the operating range of the heat fluxes was extended. When the heat flux reached 161.1 W/cm^2, the fin efficiency was up to 93%. For the IFHP, the best filling ratio and inclination angle are 30% and $\theta = 0°$, respectively, at which the best heat performance was achieved, and the minimum total thermal resistance was 0.33 K/W.
- A relative temperature uniformity coefficient β was introduced to study how the temperature uniformity on the fin base surface and the evaporator bottom plate surface varied with heat flux. When the heat flux reached 117 W/cm^2, β yielded a maximum value of approximately 0.17 for the fin base surface, and 0.09 for the evaporator bottom plate surface.
- Cooling methods and inclination angles had certain effects on the heat performance of the IFHP. In terms of cooling the heat sink, water cooling was more efficient than air cooling. In the case of water cooling, the best heat performance was achieved at $\theta = 0°$, where the minimum total thermal resistance was 0.12 K/W, and the heat flux reached up to 350 W/cm^2 without being close to drying out.

Acknowledgements

This work is supported by the National Natural Science Foundation of China (51276061), the Key Project of Natural Science Foundation of China (51436004), and Foundation of CNNC Key Laboratory on Nuclear Reactor Thermal Hydraulics Technology.

References

[1] M.T. North, C.T. Avedisian, Heat pipes for cooling high flux/high power semiconductor chips, ASME J. Elect. Pack. 115 (1993) 112–117.
[2] C. Oshman, B. Shi, C. Li, R. Yang, Y. Lee, G. Peterson, et al., The development of polymer-based flat heat pipes, J. Microelectromech. Syst. 20 (2011) 410–417.
[3] J.S. Chen, J.H. Chou, The length and bending angle effects on the cooling performance of flat plate heat pipes, Int. J. Heat Mass Transfer 90 (2015) 848–856.
[4] L.L. Vasiliev, Micro and miniature heat pipes-electronic component coolers, Appl. Therm. Eng. 28 (2008) 266–273.
[5] R.J. McGlen, R. Jachuck, S. Lin, Integrated thermal management techniques for high power electronic devices, Appl. Therm. Eng. 24 (2004) 1143–1156.
[6] Y.S. Ju, M. Kaviany, Y. Nam, S. Sharratt, G.S. Hwang, I. Catton, E. Fleming, P. Dussinger, Planar vapor chamber with hybrid evaporator wicks for the thermal management of high-heat-flux and high-power optoelectronic devices, Int. J. Heat Mass Transfer 60 (2013) 163–169.
[7] D.A. Benson, R.T. Mitchell, M.R. Tuck, D.W. Palmer, G.P. Peterson, Ultrahigh-capacity micromachined heat spreaders, Microscale Thermophys. Eng. 2 (1998) 21–30.
[8] R. Hopkins, A. Faghri, D. Khrustalev, Flat miniature heat pipe with micro capillary grooves, J. Heat Transfer 121 (1999) 102–109.
[9] S. Launay, V. Sartre, M.B. Mantelli, K.V. de Paiva, M. Lallemand, Investigation of a wire plate micro heat pipe array, Int. J. Therm. Sci. 43 (2004) 499–507.
[10] Y.X. Wang, G. Peterson, Analysis of wire-bonded micro heat pipe arrays, J. Thermophys. Heat Transfer 2 (2002) 346–355.
[11] K. Paiva, M. Mantelli, Theoretical thermal study of wire-plate mini heat pipes, Int. J. Heat Mass Transfer 83 (2015) 146–163.
[12] Y.X. Wang, G. Peterson, Investigation of a novel flat heat pipe, J. Heat Transfer 127 (2005) 165–170.
[13] J.H. Liou, C.W. Chang, C. Chao, S.C. Wong, Visualization and thermal resistance measurement for the sintered mesh-wick evaporator in operating flat-plate heat pipes, Int. J. Heat Mass Transfer 53 (2010) 1498–1506.
[14] Y.M. Xuan, Y.P. Hong, Q. Li, Investigation on transient behaviors of flat plate heat pipes, Exp. Therm. Fluid Sci. 28 (2004) 249–255.
[15] S.C. Wong, J.H. Liou, C.W. Chang, Evaporation resistance measurement with visualization for sintered copper-powder evaporator in operating flat-plate heat pipes, Int. J. Heat Mass Transfer 53 (2010) 3792–3798.
[16] Q. Cai, C.L. Chen, Design and test of carbon nanotube biwick structure for high-heat-flux phase change heat transfer, J. Heat Transfer 132 (2010), 052403–1–8.
[17] B.B. Chen, W. Liu, Z.C. Liu, H. Li, J.G. Yang, Experimental investigation of loop heat pipe with flat evaporator using biporous wick, Appl. Therm. Eng. 42 (2012) 34–40.
[18] X. Huang, G. Franchi, Design and fabrication of hybrid bi-modal wick structure for heat pipe application, J. Porous Mater. 15 (2008) 635–642.
[19] Z. Sun, H.H. Qiu, An asymmetrical vapor chamber with multiscale micro nanostructured surfaces, Int. Commun. Heat Mass 58 (2014) 40–44.
[20] F. Arbelaez, S. Sett, R.L. Mahajan, An experimental on the pool boiling of saturated FC-72 in highly porous aluminum metal foams, in: 34th National Heat Transfer Conference, August 20–22, 2000, Pittsburgh, Pennsylvania.
[21] M.R.S. Shirazy, L.G. Fréchette, A parametric investigation of operating limits in heat pipes using novel metal foams as wicks, in: Proceedings of ASME 2010 3rd Joint US-European Fluids Engineering Summer Meeting and 8th International Conference on Nanochannels, Microchannels, and Minichannels FEDSM-ICNMM2010, August 1–5, 2010, Montreal, Canada.
[22] X.B. Ji, J.L. Xu, A.M. Abanda, Copper foam based vapor chamber for high heat flux dissipation, Exp. Therm. Fluid Sci. 40 (2012) 93–102.
[23] Y.S. Muzychka, J.R. Culham, M.M. Yovanovich, Thermal spreading resistance of eccentric heat sources on rectangular flux channels, J. Electro. Packaging 125 (2003) 178–185.
[24] M. Mochizuki, K. Mashiko, Y. Saito, T. Nguyen, X. P. Wu, T. Nguyen, V. Wuttijumnong, Thermal management in high performance computers by use of heat pipes and vapor chambers, Keynote Lecture, in: Proceedings of the 9th International Heat Pipe Symposium, Malaysia, 2008: 39–48.
[25] M.B.H. Mantelli, F.H. Milanese, V. Michels, Vapor chamber heat sink with hollow fins, J. Braz. Soc. Mech. Sci. & Eng. 34 (2012) 233–237.
[26] J.C. Hsieh, D.T.W. Lin, H.J. Huang, T.W. Yang, An experimental study on the compatibility of acetone with aluminum flat-plate heat pipes, J. Heat Mass Transfer 50 (2014) 1525–1533.
[27] V.V. Calmidi, Transport Phenomenon in High Porosity Metal Foams PhD thesis, University of Colorado, CO., USA, 1998.
[28] G. Hansen, E. Næss, Performance of compressed nickel foam wicks for flat vertical heat pipes, Appl. Therm. Eng. 81 (2015) 359–367.
[29] H.T. Zhang, Q.L. Pan, H.Y. Zhang, Multi-scale porous copper foams as wick structures, Mater. Lett. 106 (2013) 360–362.
[30] D.T. Queheillalt, G. Carbajal, G.P. Peterson, H.N.G. Wadley, A multifunctional heat pipe sandwich panel structure, Int. J. Heat Mass Transfer 51 (2008) 312–326.
[31] J. Li, L.C. Lv, Experimental studies on a novel thin flat heat pipe heat spreader, Appl. Therm. Eng. 93 (2016) 139–146.
[32] E. Meléndez, R. Reyes, The pool boiling heat transfer enhancement from experiments with binary mixtures and porous heating covers, Exp. Therm. Fluid Sci. 30 (2006) 185–192.
[33] J.S. Go, Quantitative thermal performance evaluation of a cost-effective vapor chamber heat sink containing a metal-etched microwick structure for advanced microprocessor cooling, Sens. Actuators, A 121 (2005) 549–556.
[34] J.C. Hsieh, H.J. Huang, S.C. Shen, Experimental study of microrectangular groove structure covered with multimesh layers on performance of flat plate heat pipe for LED lighting module, Microelectron. Reliab. 52 (2012) 1071–1079.
[35] F. Kaminaga, H. Hashimoto, K. Goto, K. Matsumura, Heat transfer characteristics of evaporation and condensation in a two-phase closed thermosyphon, in: Proceedings of the International Heat Pipe Conference, Stuttgart, 1997, 1–6.
[36] A.B. Solomon, R. Roshan, W. Vincent, V.K. Karthikeyan, L.G. Asirvatham, Heat transfer performance of an anodized two-phase closed thermosyphon with refrigerant as working fluid, Int. J. Heat Mass Transfer 82 (2015) 521–529.
[37] H.K. Forster, N. Zuber, Dynamics of vapor bubbles and boiling heat transfer, AIChE J. 1 (1955) 531–535.
[38] H.S. Peng, C.L. Chen, Hybrid differential transformation and finite difference method to annular fin with temperature-dependent thermal conductivity, Int. J. Heat Mass Transfer 54 (2011) 2427–2433.